CONF-841043--3

CONF-841043--3

DE85 005709

STUDY OF SOLUTE SEGREGATION AT INTERFACES USING AUGER ELECTRON SPECTROSCOPY

C. L. White

Metals and Ceramics Division
Oak Ridge National Laboratory
Oak Ridge, Tennessee 37831

DISCLAIMER

STUDY OF SOLUTE SEGREGATION AT INTERFACES USING AUGER ELECTRON SPECTROSCOPY*

C. L. White

Metals and Ceramics Division
Oak Ridge National Laboratory
Oak Ridge, Tennessee 37831

Abstract

Interfacial segregation, often confined to within a few atomic distances of the interface, can strongly influence the processing and properties of metals and ceramics. The thinness of such solute-enriched regions can cause them to be particularly suitable for study using surface sensitive microanalytical techniques such as Auger electron spectroscopy (AES). The application of AES to studies of interfacial segregation in metals and ceramics is briefly reviewed, and several examples are presented.

I. Introduction

Trace solute elements,† often present at levels on the order of a few parts per million, can produce truly profound effects on the physical, mechanical (1) and electronic properties (2) of crystalline materials. Such effects often result from the interaction of the trace solute with crystal defects, thus affecting the energetics or kinetics of various defect controlled phenomena.

Interfaces, such as those depicted schematically in Fig. 1, can be considered to be two dimensional arrays of crystal defects. Because of

*Research sponsored by the Division of Materials Sciences, U.S. Department of Energy under contract DE-AC05-840R21400 with the Martin Marietta Energy Systems, Inc.

†We use the term "trace solute element" to include both unintentional impurities and intentional microalloying additions.

their spatial continuity and metastability,* such interfaces play particularly important roles in the processing and properties of most technologically significant materials. For example, all solid materials interact with their environment through a "free surface." Grain boundaries form continuous paths throughout polycrystalline materials along which fracture (3) or rapid mass transport can occur (4). Properties of solid-solid interphase boundaries are intimately involved in such diverse materials phenomena as phase transformations (5), oxidation (6), brazing (7), soldering (8), and ductile failure (9).

Solute enrichment at interfaces, in the absence of second phase formation, is called segregation (10). Although segregation can result from non-equilibrium driving forces, such as defect fluxes due to quenching or radiation damage (11), much experimentally observed segregation appears to be explained by an equilibrium attraction between the solute and the interface. The physical basis for such an attraction stems from the lattice defect energy associated with displacement of a solvent atom in the bulk lattice with a solute atom, coupled with the lattice distortion and excess energy associated with the interface (12–15). It appears that significant reductions in the defect energy of a crystalline system often result from the exchange of a solute atom on a bulk lattice site, with a solvent atom on a distorted interfacial site. As a result of such attractions, interfacial regions may contain solute concentrations several orders of magnitude higher than the bulk crystals. Segregation can, in turn, strongly influence many interfacial properties upon which the processing and performance of materials depend (10).

*We refer to interfaces as "metastable" defects because their formation is generally thermodynamically unfavorable, and is usually a result of external physical constraints (e.g. finite size in the case of free surfaces) or processing history (e.g. independent nucleation of grains to prevent formation of single crystal material) that prevents a true minimum free energy configuration from being established.

The nature of interatomic bonding in metals is such that solute atoms more than a few atom distances away from an interface will not "sense" its presence (14). The short range of solute-interface interactions leads to segregation that extends only a few atomic distances into the adjacent crystal(s). The thinness of such solute-enriched regions is the principal reason why surface sensitive microanalytical techniques such as Auger electron spectroscopy (AES) are particularly useful for the study of segregation in metals.

The ionic character of many ceramic materials leads to additional factors that may be important in determining the thickness of a solute enriched interfacial region (15). If the formation energy of cation vacancies is different from that for anion vacancies at interfaces, the resulting net charge on the interface will result in a "space charge" of vacancies of the opposite sign in the crystal(s) adjacent to the interface. The space charge region may extend considerably farther into the bulk crystals than do the solute-interface interactions typical of non-ionic crystals. To the extent, then, that the space charge may contribute to a solute-interface binding energy, one might expect somewhat thicker (perhaps 10^2 atomic distances) solute-enriched regions at interfaces. Most direct observations of interfacial segregation in ceramics so far seem to indicate that solute-enriched zones are quite thin, and consistent with interactions qualitatively similar to those in metals (16).

There are two distinct ways in which a thin solute enriched zone at an interface can be analysed. If the interface can be conveniently viewed "edge-on" [Fig. 2(*a*)], a small diameter probe can be placed on the interface, and the resulting analysis compared with one away from the interface. An important requirement for this mode of analysis is that the probe

diameter not be much greater than the thickness of the solute-enriched zone. In recent years, techniques such as scanning transmission electron microscopy (STEM) in combination with x-ray fluorescence analysis (XFA) or electron energy loss spectroscopy (EELS), as well as imaging atom probe-field ion microscopy (IAP-FIM) have been refined to the point where they can sometimes be useful for analyzing of interfacial segregation in this mode.

If the interface to be analysed is (or can be exposed as ...) an external free surface, then a variety of "surface sensitive" analytical techniques may be useful in studying interfacial segregation [Fig. 2(*b*)]. The primary requirement for this approach to interfacial analysis is that the depth of analysis not be much greater than the thickness of the solute-enriched zone at the interface. This mode of analysis forms the basis for the application of Auger electron spectroscopy (AES), x-ray photoelectron spectroscopy (XPS), ion scattering spectroscopy (ISS), and secondary ion mass spectroscopy (SIMS) to the study of interfacial segregation (17). Of these surface sensitive techniques, AES has found the broadest application to the study of interfacial segregation in polycrystalline materials.

In this paper, we briefly review the principles and application of AES to the study of interfacial segregation in both metal and ceramics systems. Special problems associated with analysis of ceramics as well as advantages and disadvantages of AES relative to other microanalytical techniques will be discussed. Several examples of studies on oxide and non-oxide ceramics are presented.

II. Physical Basis of Auger Electron Spectroscopy

(1) The Auger Transition

When a core level vacancy is created in the electronic structure of an atom, it will relax to a lower energy state via transition of an outer shell electron to fill the core level vacancy as illustrated schematically in Fig. 3(a). The energy associated with this transition may be released in two ways. If the energy associated with the transition is greater than about 2 keV, there is a significant probability that a characteristic x-ray will be emitted [Fig. 3(b)]. This is the basis for elemental analysis using x-ray fluorescence in scanning electron microscopes and electron microprobes.

If the energy associated with the transition of Fig. 3(a) is less than about 2 keV, there is a high probability that an outer shell electron will be ejected from the atom [Fig. 3(c)] with a characteristic energy E_A. This mechanism was discovered in 1925 by P. Auger (18) and is called an Auger transition. All solid elements except hydrogen and helium exhibit observable Auger transitions, and the lighter elements tend to exhibit stronger transitions than do heavy elements. The particular transition in Fig. 3(a) is named a "KL_IL_{II} transition," according to the energy levels participating in the process. The measured energy of the Auger electron, E_A, is given by:

$$E_A = E_K - \acute{E}_{LI} - \acute{E}_{LII} - \Phi_a \qquad (1)$$

where $\acute{E}_{LI}$ and $\acute{E}_{LII}$ differ slightly from ground state binding energies of the LI and LII levels due to shifts resulting from prior ionization of the K shell, and Φ_a is the electron work function of the electron energy analyser (19).

The energy of the Auger electron is characteristic of the electronic structure of the element, which forms the basis for elemental identification in AES. Of many possible combinations of energy levels that might give rise to Auger transitions, only a limited number are actually observed to occur with any significant intensity. The energies of possible Auger transitions for all elements have been calculated and catalogued by Coghlan and Clausing (20) and may be compared with the experimentally observed energies and intensities for electron excited Auger peaks for most elements from the work of Davis and coworkers (21).

(2) The Secondary Electron Spectrum

Although Auger transitions can result from both ion and electromagnetic radiation, electron excited Auger transitions are by far the most commonly used in AES analysis of interfacial segregation. The energy of the exciting electron beam (primary beam), E_p must be sufficient to ionize the atom [Fig. 3(a)], and the ionization cross section is reported to be maximum for primary beam energies approximately three times the ionization threshold (i.e. E_K in Fig. 3) (22). This cross section increases rapidly in the range $E_K < 3E_K$. Depending on the energy of the Auger transitions being observed, as well as requirements for focusing the primary beam, values of E_p in the range from 1.5 - 10 keV are commonly employed. Although, the energy of the Auger transition is independent of E_p, the intensity of an observed Auger transition will depend upon the ionization cross section and hence upon E_p.

Curves (a) and (b) in Fig. 4 show the secondary electron spectrum from a nickel alloy excited by a 1500 eV electron beam. Because of the energy dependent "pass bandwidth" of the cylindrical mirror analyser (CMA)

used to acquire this spectrum, the signal is proportional to $E \cdot N(E)$, where $N(E)$ is the energy distribution of secondary electrons. The large number of electrons having energies less than ~50 eV are generally called "true secondary" electrons, and comprise the majority of the electrons emitted from the surface. Variations in secondary electron emission due to orientation, crystallographic effects, and surface roughness are responsible for the contrast in conventional scanning electron microscopy. At the high energy end of the spectrum, the large peak at 1500 eV is due to elastically reflected electrons from the incident primary electron beam. In between the true secondaries, and the elastic peak, is a relatively smooth background upon which small peaks due to Auger transitions from C, O, and Ni are indicated. In order to make these Auger peaks more easily visible, the energy spectrum is often differentiated as shown in curve (*b*). The peak-to-peak intensity of Auger peaks in the differentiated spectrum is generally taken to be proportional to the concentration of the element in the volume of material being excited by the primary beam. This assumption has been shown by Weber and Johnson (23) to be reasonable for situations where the peak shape is not significantly changed over the concentration range of interest.

(3) Surface Sensitivity of AES

Primary electron beams of several keV can excite Auger transitions many tens (or even hundreds) of atom layers deep into a solid material. Most elements exhibit strong Auger transitions having energies of less than 1000 eV, however, and these characteristic electrons can travel only a few atomic distances in a solid before undergoing inelastic scattering and losing their characteristic energy (see Fig. 5) (24,25). Those electrons that do exhibit the characteristic energy, can therefore be

assumed to originate within the top few atom layers of a specimen surface. It is the limited inelastic mean free path of low energy electrons that permits AES to detect only the top few atom layers on a specimen surface.

(4) Quantitative Analysis - Without Segregation

Figure 6 shows an Auger spectrum from an experimental cast of austenitic stainless steel, whose composition was 69.9 at. % Fe, 13.6 at. % Ni, and 16.5 at. % Cr as determined by wet chemical analysis (26). The spectrum was obtained from a region of ductile transgranular fracture, and should represent an analysis of the bulk alloy. Quantitative analysis of this spectrum could be attempted in several ways, but the most practical involves comparison with standards of known composition (21,27). Perhaps the most widely used version of this approach involves the use of sensitivity factors from pure spectra of elemental standards and pure chemical compounds. At least two sets of such standard spectra, which simply represent spectra from pure elements and known compounds obtained using identical experimental parameters, have been published (21,28). Peak intensities from different standard spectra are directly comparable, so that relative sensitivities for the various peaks of several elements can be established. These relative sensitivities can then be used to evaluate relative concentrations in spectra from multicomponent specimens of unknown composition. In the case of the Fe-Ni-Cr alloy in Fig. 6, the use of sensitivity factors from the published standard spectra yields a composition of 68.5 at. % Fe, 14.6 at. % Ni, and 16.9 at. % Cr, in good agreement with the bulk analysis by wet chemistry.

If the chemical state of an element is greatly different from that for which the standard spectra were obtained, the energy, shape and sensitivity of that peak may be significantly altered. The handbook

published by Davis et al. (21) includes standard spectra from pure silicon, SiO_2, and MgO. Comparing spectra of Si and SiO_2 reveals a marked change in peak shape, a 10-20 eV shift in the major silicon Auger peaks, and a change in their sensitivity by more than a factor of two. If the SiO_2 spectrum were analysed using oxygen sensitivity factors from the MgO spectrum, and silicon sensitivity factors from pure silicon, one would estimate about 60 at. % Si rather than 33 at. % as indicated by the formula. In using sensitivity factors, therefore, one must keep in mind that their value is not independent of chemical state.

Another factor that can affect quantitative analysis of Auger spectra involves the effects of backscattered electrons such as those contributing to the elastic peak in Fig. 4. Auger transitions can be created in the near surface region by both the incoming electrons, and by electrons backscattered from underlying layers as they pass through the near surface region on their way out of a specimen. Since the efficiency of the backscattering process increases with the atomic mass of the matrix atoms, one might expect higher sensitivities for a light element in a matrix of heavy atoms. Tarng and Wehner (29) have observed an increase in the intensity of the 120 eV Mo signal (compared to pure molybdenum) by depositing a molybdenum overlayer on tungsten. The maximum signal was about 20% greater than for pure molybdenum, and occurred when the thickness of the overlayer was slightly greater than the inelastic mean free path for 120 eV electrons. Analysis of backscattering effects based on empirical correction factors for electron microprobe analysis indicates that the effect is most severe for combinations of elements having greatly different atomic numbers and should not often affect relative sensitivities by more than about 20% (27).

In cases where accurate quantitative analysis of Auger spectra is important, it is probably advisable to prepare standards with compositions similar to those in the spectrum being analyzed. Even this approach is not without difficulties, however, since once a standard specimen is prepared, an external surface having the bulk composition must be created. If a standard can be fractured transgranularly in-situ, an accurate quantitative analysis and standard spectrum can usually be obtained. If the standard fractures intergranularly, however, the exposed surface may be much different from the bulk composition (e.g. due to segregation), invalidating the standard. If the standard cannot be fractured in-situ, surface contamination from specimen preparation can sometimes be removed by sputter etching [see Sec. III(3)]. Unfortunately sputter etching does not always remove all elements with equal efficiency. Such "preferential sputtering" can lead to enrichment or depletion of components on the surface of the standard, again invalidating the standard. In-situ mechanical removal of surface contamination (eg. filing or scraping) has also been used occasionally. Transfer of material from the removal tool to the specimen is obviously a potential problem with this method, especially if the specimen is hard or reacts with the tool.

(5) Quantitative Analysis - With Segregation

If a specimen is not compositionally uniform in the direction normal to the surface being analysed, translating information from the Auger spectrum into a quantitative estimate of the surface composition involves some additional complications. Perhaps the first of these complications involves definition of what we mean by composition (30). Although the analysis depth of AES is small, it is finite, and therefore any observed Auger signal represents an average of the solute concentration profile

over that analysis depth.* Since the concentration of strongly segregating solutes may change by several orders of magnitude over this depth, the average concentration can depend strongly on the exact value of analysis depth and hence the energy of the Auger transitions employed in the analysis. For this reason, even when bulk standards are used as described in the previous section, it is advisable to base quantitative analyses on the intensities of those Auger peaks having the smallest difference in energy.

We should note that it is also possible to create standards of known surface composition by vapor- or sputter-deposition techniques. The quantity of deposited material can be monitored fairly accurately, and if the deposition is known to be uniform, and not to form islands or precipitates on the surface, then such standards can form the basis for accurate quantitative analysis in specimens where segregation or adsorption is known to occur. Because the effort involved in preparing standards and performing accurate quantitative analysis on segregation enriched surfaces is quite substantial, approximate or semiquantitative analyses of spectra are more often performed. Such analyses ignore most of the complications sited in this and the previous section, and therefore yield average compositions that may be significantly in error, or at least have sampling depths that are ill defined. Such analyses can still be quite useful, however, since they usually provide a value proportional (even if not equal) to the actual surface concentration of segregating solutes.

*Strictly speaking, the observed Auger signal depends on the convolution of the concentration profile with the depth dependent escape probability for the characteristic electron. This will bias the average toward the composition near the surface, but such refinements are beyond the scope of the present discussion.

The center spectrum shown in Fig. 6 was obtained from the surface of an internal grain boundary cavity formed during creep at elevated temperatures. Although the bulk sulfur concentration in this alloy is less than 10 at. ppm, a rough estimate of sulfur concentration on the cavity surface is 23 at. % in the top few atom layers probed by AES. Following removal of less than ten atom layers by inert ion sputter etching [see Sec. III(3)] this sulfur is below the detectability limit, illustrating the dramatic change in composition that can occur over a few atomic distances near interfaces.

III. Experimental Aspects of AES for the Study of Interfacial Segregation

(1) Vacuum Requirements

Auger electron spectroscopy is a surface sensitive technique, and in order to be useful in studying interfacial segregation, the surface being analysed must remain sensibly unaltered during the course of the AES analysis which may require several hours for complex inhomogeneous surfaces.

If we consider the interaction of gas at low pressure, P, with a clean metal surface, we find that the time, t, required to absorb an atom layer of gas molecules is given approximately as (19):

$$t = \frac{10^{-6}}{S \cdot P} \text{ [torr.s]}$$

where S is the probability that an incident gas molecule will stick on the surface. Since S is frequently close to unity, the pressure required to get t approximately one hour is on the order of 10^{-10} torr. Such stringent vacuum requirements constitute one of the principal experimental constraints associated with the application of AES to studies of interfacial segregation. Vacuum systems in which AES analyses are carried out are generally

pumped using getter ion pumps with supplemental titanium sublimation pumps. Since neither of the above pumps will operate well at pressures above 10^{-3} torr, rough pumping is usually accomplished with liquid nitrogen cooled sorption pumps. Alternative pumping arrangements using turbomolecular pumps, or well trapped and baffled diffusion pumps are occasionally employed, but extreme care must be exercised to avoid contamination of the analysis chamber with pump fluid vapors.

Vacuum system components are usually made of austenitic stainless steel, glass, and oxide ceramics. Flanged connections are generally sealed with metal gaskets (usually Cu, Au, or Al) that are deformed during sealing to insure a vacuum tight closure. High vapor pressure metals (e.g. Cd, Zn, or As as might be found in solder, braze metal, or plating) and most plastics and rubbers are usually avoided because they can evaporate or decompose at temperatures and pressures routinely encountered in analysis chamber, sometimes condensing in cooler parts of the vacuum chamber and creating persistent sources of contamination and outgassing. Certain polyamide materials can be used when system bake out temperatures (see below) are kept below 250°C.

Following exposure to atmospheric pressure, a vacuum chamber may pump down very slowly at pressures below 10^{-6} or 10^{-7} torr, due to desorption of gases (primarily water vapor) from the chamber walls. Heating or "baking" the vacuum system to at least 200°C is often helpful in desorbing gases from surfaces exposed to the vacuum. If significant quantities of hydrogen are dissolved in the bulk of any system components, higher temperature outgassing may be required.

Because a "bake out," and a total elapsed time greater than 24 h is often required to achieve a 10^{-10} torr vacuum prior to AES analysis,

vacuum introduction locks have become popular accessories for AES analysis chambers. Design details vary widely, and some retain the traditional "all metal and glass" construction while others introduce viton or polyamide seals, and mechanical/turbomolecular pumped locks which can compromise the ultimate achievable base pressure of the analysis chamber. The use of these non-metal or glass components, and alternate pumping on the lock permits a much greater degree of automation and speed in the introduction system, however, and may be warrented in cases where a slight increase in contamination can be tolerated in return for significantly increased specimen throughput.

(2) Electron Energy Analysers and Electron Guns

In order to detect Auger electrons, the electrons from an excited surface must be energy-analysed. Several types of electron energy analysers have been used for this purpose, and for a detailed discussion the interested reader is referred to a book by Ertl and Küppers (19). The most common type of analyser currently in use is the cylindrical mirror analyser (CMA) shown in Fig. 7. When the specimen is positioned properly in the focal point of the analyser, a negative voltage applied to the outer cylinder by the CMA control defines the range of electron energies $[E_p - (\Delta E_p/2)] < E < [E_p + (\Delta E_p/2)]$ that can enter the analyser* and be deflected through the rear slits onto an electron multiplier (dashed curve). Because $\Delta E_p/E_p$ is a constant for the CMA, the current passing through the CMA is proportional to $E \cdot N(E)$. By recording this current as a function of CMA control voltage, a plot of $E \cdot N(E)$ versus E is generated.

*Here E_p is defined as the nominal pass energy of the CMA, and ΔE_p is its (energy dependent) pass band width.

Some CMAs are equipped with an adjustable aperture at the rear focal point that defines $(\Delta E_p/E_p)$, allowing the energy resolution to be adjusted according to the needs of a given analysis. For example, a small ΔE_p (high energy resolution) might be desired to resolve two overlapping peaks from different elements at the expense of overall sensitivity. On the other hand, low energy resolution (large ΔE_p) might be accepted in order to maximize signal while analysing for small concentrations of an element whose Auger peak is well separated from others in the spectrum. A typical range of $(\Delta E_p/E_p)$ values in a CMA is 0.003 to 0.012.

The electrons passing through the CMA generally strike the input of an electron multiplier, which amplifies the signal. The gain of the electron multiplier is controlled by a high voltage power supply, and with use, the voltage required to get a given gain increases. The gain of the electron multiplier can also depend on the energy of the incoming electrons, especially in the range below 200 eV, so that details of the $E \cdot N(E)$ spectrum may not be reflected accurately by its output (21). Such factors can be worrisome if absolute values of $N(E)$ are needed; however, they can usually be adequately compensated-for in studies involving comparison of unknown specimens with standards.

Of the various types of analysers available, the CMA has two features that make it desirable for analysis of rough or inhomogeneous surfaces. First, it is possible to mount an electron gun on the axis of the CMA, so that the primary electron beam strikes the surface at (nominally) normal incidence. This is an advantage for analysis of rough surfaces (e.g. fracture surfaces) since a grazing incidence electron beam may be shadowed from certain areas of such surfaces. The second significant advantage of the CMA is that it accepts secondary electrons symmetrically about the CMA

axis. Again this minimizes the likelihood that some portion of a rough surface will be unfavorably oriented for analysis. Use of a CMA with a coaxial electron gun, therefore, maximizes both the probability that any given spot on a surface can be excited by the primary beam, and that the resulting secondary electron spectrum can be analysed.

The electron gun used in AES analysis should provide an electron beam having sufficient energy to excite the desired Auger transitions, and sufficient primary beam current to provide a detectable current of Auger electrons. As noted previously, primary beam energies from 1.5 keV to 10 keV are fairly common, and beam currents ranging from less than 1 nA to hundreds of micro-Amperes are used depending on the specific type of analyser and detection system employed.

It is also advantageous if the electron beam can be focussed to a small diameter, and electronically positioned on the specimen surface. This permits the beam to be rastered over the surface as in a scanning electron microscope (SEM), and images of the surface to be generated using the secondary electron emission or the absorbed sample current to modulate the image brightness. A secondary electron image of the austenitic steel in Fig. 6 is shown in (*b*). This image was obtained during AES analysis using an electron beam having <1 μm diameter. Figure 6(*a*) shows a conventional SEM image of the fracture surface obtained after the specimen was removed from the AES system.

If the intensity of an Auger peak is used to modulate the image brightness, a map of the elemental distribution on the surface can be generated. The details of how the Auger peak intensity is measured for such maps vary according to the sophistication of the detection system, and can affect the extent to which brightness of such "Auger Maps" are

influenced by surface topography. Modern computer controlled analysers and data acquisition systems permit data acquisition and analysis routines to be applied at each point of a digital elemental map, which can significantly reduce topographical effects. Figure 6(*a*) shows a sulfur map over the field of view shown in Fig. 6(*b*). The sulfur rich regions clearly correspond to the rounded depressions in Fig. 6(*b*), which are the surfaces of grain boundary cavities created during creep, then exposed fracturing the specimen inside the AES analysis chamber. The sulfur poor regions are areas where the intercavity ligaments failed in a ductile transgranular fashion.

(3) In-Situ Specimen Manipulation and Preparation

Specimen surfaces that have been exposed to laboratory or service environments generally have extensive oxygen or carbon adsorption, and in the case of reactive specimens, they may have films of oxide or other reaction products. Unless the specimen interaction with the laboratory or service environment is of specific interest, it is necessary to produce or expose the interface of interest in the AES system in a controlled way so that it can be analyzed under UHV conditions. This often involves fracturing the specimen to expose an internal interface, or removal of surface contamination followed by a specimen treatment to produce the surface desired for analysis. Examples of such operations are briefly outlined below.

If the interface of interest is not an external interface, then it must be exposed as an external interface for AES analysis. This can often be accomplished by fracturing the specimen along the interface, then positioning the fracture surface in front of the analyser for analysis.

The fracture must generally take place under Ultra High Vacuum (UHV) and the specimen must remain under UHV until the analysis is complete. Many devices have been used to fracture specimens, some of which can be cooled with liquid nitrogen to induce brittle fracture, while others permit heating to induce failure via creep cavitation and cracking. Specimens are often fractured in bending, but sometimes uniaxial tension is found to be helpful in inducing fracture along the desired interface. If the specimen does not fail primarily along the desired interface, or if the fracture surface exposes several types of interfaces (e.g. grain boundaries, interphase boundaries, and internal free surfaces), then the capability to image the fracture surface and analyse small areas as described in Section III(1) becomes extremely important. When fracture is not possible, other methods of exposing internal interfaces are occasionally successful. Lindfors has summarized variations of angle lapping or taper sectioning that might be satisfactory in certain cases (31).

If the interface of interest is already an external free surface, it is frequently desirable to remove contamination from the ex-situ specimen preparation. This is most often accomplished by inert ion sputtering, which involves bombarding the surface with inert gas ions, such as argon or xenon, having energies of several keV. Sputter profiling, which involves monitoring Auger signals of one or more elements as a function of sputtering time, is also used to obtain information regarding the composition profile in the direction normal to the interface being analysed. Wehner has reviewed the physics of the sputtering process as it is applied in surface analysis (32), and the interested reader is referred to this work for a more detailed discussion of the subject. From the standpoint

of AES studies, it is important to note that the sputter yield (i.e. the number of surface atoms removed per incident gas ion) can vary significantly from material to material, and depends on the angle of incidence of incoming ion beam to the surface normal, as well as the energy of the incident ions. If the sputter yields for two components in a specimen are different, sputtering can result in surface enrichment of the component having the lower yield. There is some evidence that preferential sputtering effects are aggravated at extremely low ion energies (29). Finally, it should be pointed out that although sputtering is sometimes described as though it is a layer by layer removal process, it is really a stochastic process. Ejection of sputtered atoms from the near surface region often involves a succession of collisions. Gas ions may be implanted in the near surface region, and mixing and lattice damage can also occur. Any impurities present in the sputtering gas may also be implanted in the surface, resulting in some contamination of the sputtered surface. The carbon and oxygen peaks on the sputtered cavity surface of Fig. 6 probably result from CO, H_2O, and CH_4 residual gases incorporated into the ion beam. As a result of these effects, "sputter cleaning" may sometimes fail to yield a perfectly clean surface having the bulk composition. Furthermore, "sputter profiling" may yield information relating to (but perhaps not exactly describing) the actual composition profile normal to a segregation enriched surface.

Once cleaned, it is sometimes desirable to heat the specimen, or expose it to a controlled environment prior to analysis. Heating can be accomplished by passing a current through the specimen, by contact with a heated substrate, by electron bombardment, or by radiation. Some care must be exercised to avoid excessive distortion of the Auger spectrum due

to induced magnetic fields from electric currents. This can be minimized by proper arrangement of the conductors, and in some cases rapidly alternating heating and data acquisition cycles can be employed (33).

Exposure of a cleaned specimen to controlled gaseous environments is usually accomplished by transferring the specimen to an adjacent environmental cell. The environmental cell may be as simple as a low pressure gas or plasma (34), or it may be as complex as a large fusion experiment (35). In either case, some mechanism for transporting the specimen from the analysis chamber under vacuum is required. In some circumstances, specimens have been exposed to gaseous environments during AES analysis by directing the gas onto the surface of interest with small capillaries and differentially pumping the analysis region (35).

Figure 8 shows a modified version of the commercial AES system of Fig. 7. The CMA incorporates a coaxial scanning electron gun capable of providing analysis on spots as small as 200 nm. This system is fitted with a normal incidence sputtering gun for etching rough fracture surfaces as well as a grazing incidence (differentially pumped) ion gun for simultaneous sputtering and AES analysis. A fracture and introduction system (FAIS) is joined to the AES analysis chamber with an all-metal valve separating the two, so that the FAIS may be vented to atmospheric pressure for specimen loading while keeping the analysis chamber under UHV. This particular FAIS permits specimens to be fractured in tension (with resistance heating if desired) then transported to the analysis chamber using a rack-and-pinion driven carriage. The fractured specimen and specimen holder can then be transferred from the carriage to the specimen carousel using the X-Y-Z motion of the specimen stage.

(4) Problems Associated with the Study of Ceramics.

AES analysis of ceramics and non-metals sometimes involves complications beyond those typically encountered in analysis of metallic materials. Perhaps the most significant of these problems involves charging due to poor electrical conductivity of the specimen.

The electron current that is incident on the specimen via the primary electron beam must leave the specimen in order to avoid charge buildup (36). One mechanism by which electrons leave the specimen is secondary electron emission. The ratio, δ, of incident electron current to secondary electron current is called the secondary electron emission coefficient. If $\delta > 1$ (i.e. the secondary electron current leaving the surface is greater than the incident primary beam current) then electrons must be supplied to avoid buildup of a positive charge on the specimen. Conversely, if $\delta < 1$, electrons must be bled from the specimen to avoid build up of a negative charge. Since metallic specimens are normally in good electrical contact with the system ground, charge buildup is not a problem. If a highly insulating ceramic is analysed, however, charge buildup near the point of impact for the electron beam can cause the shifts in the observed energies of Auger peaks. If the resulting potential on the surface is relatively uniform and static, the measured spectrum may simply be shifted in energy, permitting relatively straightforward interpretation.

If the charge buildup results in a spatially non-uniform potential on the specimen, Auger peaks from different areas will be shifted by different amounts leading to broadened or multiple peaks from a single transition (37). Such local potentials may also vary with time due to buildup and bleed-off of charge. These two effects can combine to yield measured spectra that are virtually uninterpretable (see Fig. 9).

Because δ depends upon many factors, specimen charging can sometimes be controlled or eliminated by varying beam current, beam energy or specimen orientation with respect to the primary beam. Unfortunately, there seems to be little in the way of general "rules of thumb" to guide efforts to minimize charging; however, use of a grazing incidence primary electron beam has been reported to be beneficial (38). Minimizing beam current and beam voltage is also useful in the author's experience, but others have reported the opposite approach to be beneficial (39). Other measures such as wrapping the specimen in a conducting wire mesh, or depositing a thin conductive film can sometimes alleviate charging problems at the expense of complicating interpretation of the resulting spectra (38).

In addition to charging effects, the electron beam can alter the specimen surface through heating or electron beam induced desorption (EBID) effects. Heating effects have been reported for glasses (40) and fly ash particles (38) where the intensity of Auger signals was observed to vary with time, presumably due to migration and desorption under the electron beam. Sometimes such effects can be used to advantage, as in EBID studies of adsorbed species from a $Pt-Al_2O_3$ catalyst where desorbed ions were detected with a mass spectrometer (41).

IV. Applications of AES in Metals and Ceramics

AES has been applied extensively to studies of interfacial phenomena in both metals and ceramics. Several examples from the authors experience are briefly described in the following paragraphs.

(1) Impurity Effects in Creep Cavitation

Certain residual impurities (e.g. sulfur, antimony, and tin) have long been known to aggravate creep cavitation at metal grain boundaries,

causing premature, low-ductility failures. Because these impurities are known to be "interfacially active" (i.e. they segregate strongly to interfaces) early investigators suspected that their harmful effects occurred through their segregation to grain boundaries and/or to the surfaces of creep cavities that formed on them. Since the availability of high spatial resolution AES, a number of studies have shown convincingly that such segregation does occur. There has also been some progress in defining the mechanisms by which this segregation influences cavitation, however insufficient knowledge concerning effects of segregants on interfacial mass transport and grain boundary sliding has been a major obstcale in this effort. One important contribution of AES to these studies has been its ability to examine creep cavity surfaces in alloys not having unusually high concentrations (as determined by conventional bulk chemical analysis) of harmful impurities. The results in Fig. 6 are representative of a fairly high purity, experimental cast of austenitic stainless steel that exhibited rather extensive creep cavitation (26). In this case, extensive sulfur segregation to creep cavity surfaces was observed in spite of a bulk sulfur content less than 10 at. ppm. We should also note that creep cavitation was eliminated completely in a companion alloy to which 0.1 wt. % Ti was added, illustrating the profound beneficial effect that small alloying additions can have.

(2) Exposure of α-SiC to a Steel Soaking Pit Environment

During the course of evaluating a number of ceramic materials for applications in high temperature heat exchangers in steel soaking pits, slag buildup was noted on the outer surface of some sintered α-SiC that had been exposed to the soaking pit environment for ~800 h at ~1250°C (42).

In an effort to better understand the effects of the soaking pit environment on the α-SiC, a number of microanalytical tools, including AES were used to investigate exposed and control materials.

Figure 10 shows optical micrographs of α-SiC tubes that were exposed to a steel soaking pit environment at 1250°C for 800 h (42). Large angular pores, which were present near the outer surface of the as-received tubes, were also observed in the secondary electron detector (SED) image of the fracture surface from the exposed tubes (see Fig. 11). Elemental Auger maps over the field of view in this SED image indicate depletion of carbon and enrichment of oxygen in the near surface region. Mapping of boron (added at trace levels to promote sintering) showed some evidence of boron enrichment on the surfaces of pores far enough from the outer surface to be unaffected by oxygen penetration. This indication was confirmed by obtaining Auger spectra from the cavity surface and an adjacent area as indicated in Fig. 11.

The residual gas analyser (RGA) spectra in Fig. 12 illustrate additional information that can sometime be obtained during the course of AES analysis. A momentary pressure increase was noticed during fracture of the first α-SiC in Fig. 11, so an additional specimen was fractured while recording the RGA output. Comparison of the resulting spectrum with control spectra indicate that argon is released during fracture. The tubes were sintered in an argon atmosphere, and argon is thought to have been trapped in the residual porosity (~2%).

(3) Examination of Ceramic/Metal Braze Joints

The wetting of ceramics by liquid metals, and the strength of metal-ceramic interfaces have broad significance in the processing, fabrication and performance of materials for advanced power generation, microelectronics and chemical processing technologies.

Figure 13(*a*) and (*b*) show SED images of a fractured braze joint between two Al_2O_3 coupons (43). The braze metal was Ag-28% Cu-4% Ti-0.5% Ni, and the joint was prepared by heating to 1160°C for 5 min. in a vacuum induction furnace. Only the upper portion of the surface in Fig. 13(*a*) was actually wetted by the braze metal, and the lower unwetted portion was covered with a thin layer of carbon in the as-fractured condition.

Spectra from the wetted area after fracture showed only aluminum and oxygen peaks, indicating that the joint failed on the Al_2O_3 side of the interface. After sputter etching the surface to remove ≈13 nm, the underlying braze metal began to appear. Curve *A* in Fig. 13(*c*) shows a spectrum from a region where the fracture exposed the underlying Al_2O_3 substrate. Curves *B* and *C* show spectra from the exposed braze metal at locations indicated in Fig. 13(*b*). Perhaps the most interesting observation from these results is that the braze metal just inside the ceramic-metal interface is mostly titanium and not silver, as might be expected from the nominal composition of the braze metal. The spatial distribution of Cu, Ti, and O are shown in the Auger maps of Fig. 14(*b*), (*c*), and (*d*). While far from telling a complete story about metal-ceramic interactions in brazed joints, these results indicate that important new information concerning the composition at the metal-ceramic interface can be obtained using AES.

V. Summary

Auger electron spectroscopy is a powerful and versatile tool for the study of interfacial composition in cases where the interface can be obtained as an external free surface. Its usefulness derives from the

fact that it probes only the top few atom layers on a surface and that it is just these top few atom layers that are often greatly different in compositon from the bulk material. Through the use of appropriate standards, the technique can be made quantitative; however, the effort required for careful quantitative analysis is usually substantial, and semiquantitative evaluation of AES results is often adequate.

Electron-excited AES can achieve spatial resolutions down to a tens of nanometers which is better than any of the other available surface sensitive techniques. It is also nominally non-destructive on most specimens. If sensitivity to very small concentrations, or detection of hydrogen or helium is important then SIMS may offer advantages over AES. If information regarding the chemical state of segregant and matrix species is important, then XPS be preferred. If even the shallow analysis depth of AES is not adequate to resolve details of interfacial chemistry, the "top" atom layer sensitivity of ISS can be useful. While each of these techniques offers its own set of advantages and disadvantages, AES is probably the most widely applied, and generally the technique of choice if only a single one can be selected.

References

1. "Residuals, Additives and Materials Properties;" pp. 7–341 in Proceedings of the International Conference, *Phil. Trans. R. Soc. Land. A*, 295 (1980).

2. C. Kittel, "Introduction to Solid State Physics", 3 ed., Wiley, 1968; pp. 308–30.

3. C. L. White; pp. 141–70 in Aluminum-Lithium Alloys. Edited by T. H. Sanders, Jr., and E. A. Starke, Jr. TMS-AIME, 1981.

4. G. Martin and B. Perraillon; pp. 239–76 in Grain Boundary Structure and Kinetics. Edited by R. W. Balluff. ASM, 1980.

5. W. C. Johnson, C. L. White, P. E. Marth, P. K. Ruf, S. M. Tuominen, K. D. Wade, K. C. Russell, and H. I. Aaronson, "Influence of Crystallography on Aspects of Solid-Solid Nucleation Therory," *Met. Trans. A*, 6A 911–19 (1975).

6. R. Hales, A. C. Hills, and R. K. Wild, "The Oxidation of Nickel at Reduced Pressures," *Corrosion Sci.*, 13 325–36 (1973).

7. P. M. Scott, M. Nicholas, and B. Devar, "The Wetting and Bonding of Diamonds by Copper-Base Binary Alloys," *J. Mater. Sci.*, 10 1833–40 (1975).

8. C. Lea; pp. 467–70 in Proceedings of the 8th International Vacuum Congress, Vol. II - Vacuum Technology and Vacuum Metallurgy.

9. A. S. Tetelman and A. J. McEvily, Jr., "Fracture of Structual Materials," Wiley, 1967; pp. 215–22.

10. W. C. Johnson and J. M. Blakely (Eds.), "Interfacial Segregation," American Society for Metals, 1979.

11. H. Wiedersich and P. R. Okamoto, pp. 405–32 in ref. (10).

12. E. D. Hondros and M. P. Seah, "The Theory of Grain Boundary Segregation in Terms of Surface Adsorption Analogues," *Met. Trans.*, 8A 1363–71 (1977).

13. M. Guttman, "Grain Boundary Segregation, Two Dimensional Compound Formation and Precipitation,", *Met. Trans.*, 8A 1383–1401 (1977).

14. C. L. White and W. A. Coghlan, "The Spectrum of Binding Energies Approach to Grain Boundary Segregation," *Met. Trans.*, 8A 1403–12 (1977).

15. M. F. Yan, R. M. Cannon and H. K. Bowen; pp. 255–73 in Advances in Ceramics, 6: Character of Grain Boundaries. Edited by M. F. Yan and A. H. Heuer. American Ceramic Society, 1983.

16. W. C. Johnson, "Grain Boundary Segregation in Ceramics," *Met. Trans. A*, 8A 1413–22 (1977).

17. A. Joshi in ref. 10, pp. 39–109.

18. P. Auger, "On the Photoelectric Effect," *J. Phys. Raduim*, 6 205–08 (1925).

19. G. Ertl and J. Küppers, "Low Energy Electrons and Surface Chemistry," Verlag Chemie, 1974; pp. 1–51.

20. R. E. Clausing and W. A. Coghlan, "Auger Catalog: Calculated Transition Energies Listed by Energy and Element," *Atomic Data*, 5 [4] 317–471 (1973).

21. L. E. Davis, N. C. MacDonald, P. W. Palmberg, G. E. Riach, and R. E. Weber, "Handbook of Auger Electron Spectroscopy," Physical Electronics Industries, Inc., 1976; pp. 1–252.

22. H. E. Bishop and J. C. Riviere, "Estimates of the Efficiencies of Production and Detection of Electron Excited Auger Emission," *J. Appl. Phys.*, 40 1740–44 (1969).

23. R. E. Weber and A. L. Johnson, "Determination of Surface Structures Using LEED and Energy Analysis of Scattered Electrons," *J. Appl. Phys.*, 40 [1] 314–18 (1969).

24. W. M. Riggs and M. J. Parker; pp. 103–58 in Methods of Surface Analysis. Edited by A. W. Czanderua. Elsevier, 1975.

25. P. Seah and W. A. Dench, "Quantitative Electron Spectroscopy of Surface - A Standard Data Base for Electron Inelastic Mean Free Free Paths in Solids," *NPL Report Chem. 82*, National Physical Laboratory, Teddington, UK, 1978.

26. C. L. White, J. H. Schneibel and M. H. Yoo; pp. 347–58 in Creep and Fracture of Engineering Material and Structures. Edited by B. Wilshire and D. R. J. Owen. Pineridge Press, 1984.

27. P. M. Hall and J. M. Morabito; pp. 392–401 in Thin Film Phenomena - Interfaces and Interactions. Edited by J. E. E. Baglin and J. M. Poate. Electrochemical Society, 1978.

28. G. E. McGuire, "Auger Electron Spectroscopy Reference Manual," Plenum, 1979.

29. M. L. Tarng and G. K. Wehner, "Escape Length of Auger Electrons," *J. Appl. Phys.*, 44 1534–1540 (1973).

30. R. L. Park, M. den Boer, and Y. Fukuda; pp. 105–25 in Characterization of Metal and Polymer Surfaces - Vol. 1: Metal Surfaces. Edited by L-H Lee. Academic Press, 1977.

31. P. A. Lindfors, "Probing Deep Interfaces," *The Phi Interface*

32. G. K. Wehner, "Methods of Surface Analysis," A. W. Czanderna, Elsevier, 1975; pp. 5–37.

33. Y.-Y. Tu and J. M. Blakely, "Blanking Resistive Heating Circuit for Auger Electron Spectroscopy Experiments," *Rev. Sci. Instrum.*, 47 [12] 1554–55 (1976).

34. R. E. Clausing, L. C. Emerson, and L. Heatherly, "Studies of Hydrogen Recycle from the Walls in Tokamaks Using a Plasma - Wall Interaction Simulator," *J. Nucl. Mater.*, 76, 77 267–72 (1978).

35. L. C. Emerson, R. E. Clausing, and L. Heatherly, "Surface Impurity Studies in the ISX-A Tokamak," *J. Vac. Sci. Technol.*, 16 [2] 766–68 (1979).

36. H. S. W. Massey and E. H. S. Burhop, "Electronic and Ionic Impact Phenomena," Oxford at the Clarendon Press, 1952; pp. 282–329.

37. T. A. Carlson, "Photoelectron and Auger Spectroscopy," Plenum, 1975; pp. 38, 39, 215, and 317.

38. S. P. Clough, Personal Communication, August 1984.

39. J. L. Hock, D. Snider, J. Kovacich and D. Lichtman, "Electron Beam Effects in AES Studies of Micron Size Insulating Particles," *Appl. Surf. Sci.*, 10 405–14 (1982).

40. F. Ohuchi, M. Ogino, P. H. Holloway, and C. G. Pantano, Jr., "Electron Beam Effects During Analysis of Glass Thin Films with Auger Electron Spectroscopy," *Surface and Interface Analysis*, 2 85–90 (1980).

41. A. Joshi and L. E. Davis, "Scanning Electron Stimulated Desorption (SESD): A Complimentary Tool for Surface Analysis." *J. Vac. Sci. Technol.*, 14 1310–1313 (1977).

42. G. C. Wei and C. L. White, "High Temperature Behavior of Pressureless-Sintered SiC in a Steel Soaking Pit Environment", *Ceram. Bull.*, 63 [7] 890–93.

43. C. L. White and A. J. Moorhead, unpublished research, Oak Ridge National Laboratory, Oak Ridge, TN, 1984.

FIGURE CAPTIONS

Fig. 1. Schematic illustration of the various types of interfaces that may exist in crystalline materials.

Fig. 2. Schematic illustration showing two distinct modes of interfacial analysis.

Fig. 3. Comparison of the Auger transition with the more familiar process of x-ray fluorescence.

Fig. 4. Secondary electron spectra from a Ni alloy, obtained using a cylindrical mirror analyser (CMA).

Fig. 5. Plot of the inelastic electron mean free path as a function of electron energy, after Riggs and Parleer (24).

Fig. 6. Conventional scanning electron micrograph (*a*), secondary electron image (*b*), sulfur map (*c*) and Auger spectra (*d*) of a creep cavitated austenitic steel that was fractured in the AES analysis chamber to expose creep cavity surfaces [*B* in (*b*)] and transgranular rupture of intercavity ligaments [*A* in (*b*)].

Fig. 7. Schematic view of a conventional AES analysis chamber incorporating a cylindrical mirror analyser (CMA) with a coaxial scanning electron gun. Curved dashed lines show the electron trajectory through the CMA.

Fig. 8. Schematic view of a more complex AES system, based on the analysis chamber in Fig. 7.

Fig. 9. Typical secondary electron spectrum from an electrically insulating specimen exhibiting charging.

Fig. 10. Optical micrograph of sintered α-SiC tubes exposed to a steel soaking pit environment.

Fig. 11. AES analysis of fractured α-SiC tubes in Fig. 10.

Fig. 12. Residual gas analyser (RGA) spectrum taken during fracture of the α-SiC tubes in Figs. 10 and 11. The bottom curve shows the RGA spectrum before fracture, and the middle spectrum illustrates the effect of striking the system without fracturing the specimen.

Fig. 13. AES analysis of a fractured ceramic/metal (Al_2O_3/71.5 Ag - 28 Cu - 4 Ti - 0.5 Ni) braze joint after removal of ≈13 nm by sputter etching. Secondary electron detector (SED) images (*a*) and (*b*) show locations where Auger spectra (*c*) were obtained.

Fig. 14. SED image and Cu, Ti, and O maps of the fractured braze joint in Fig. 13.

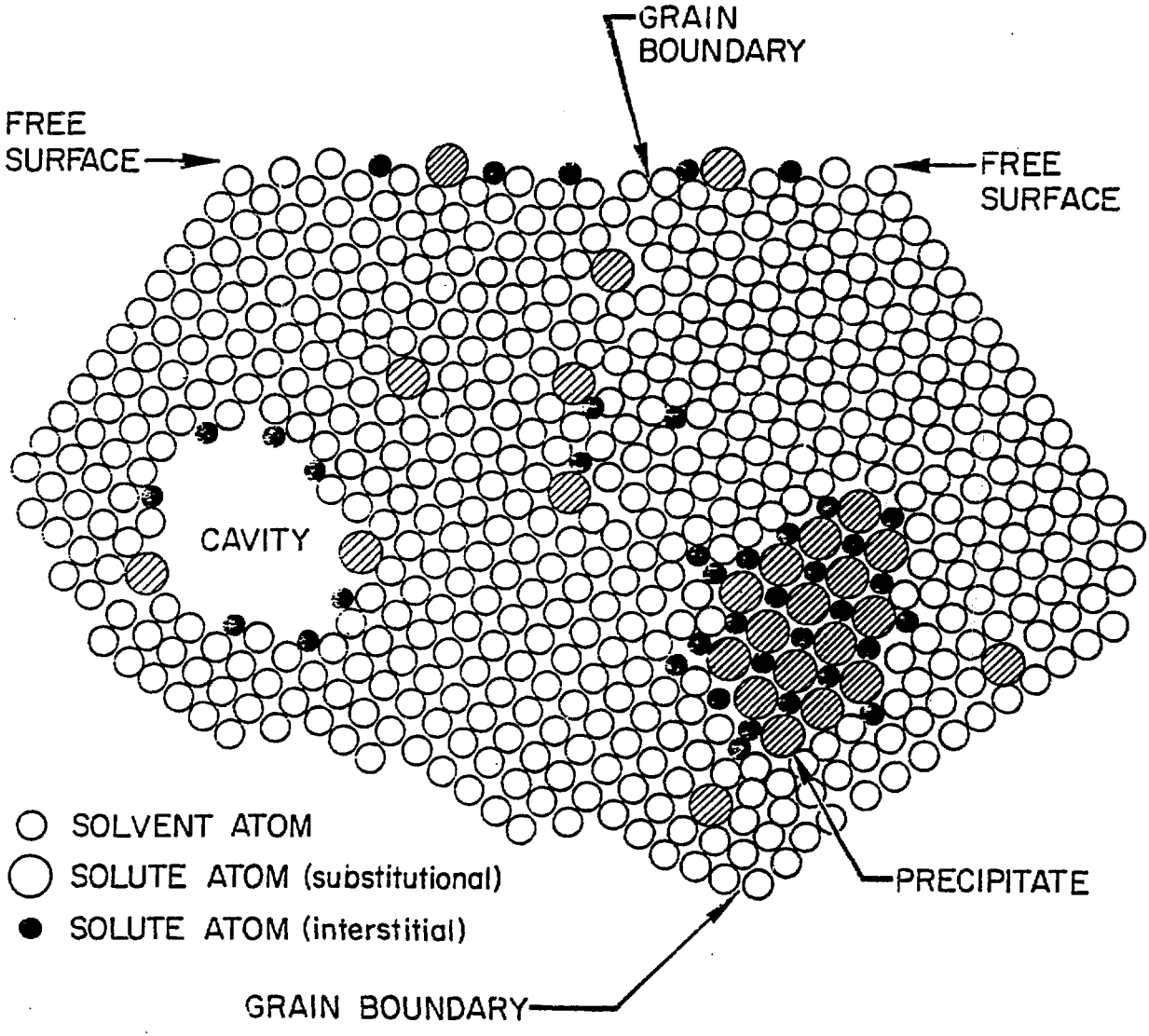

Fig. 1. Schematic illustration of the various types of interfaces that may exist in crystalline materials.

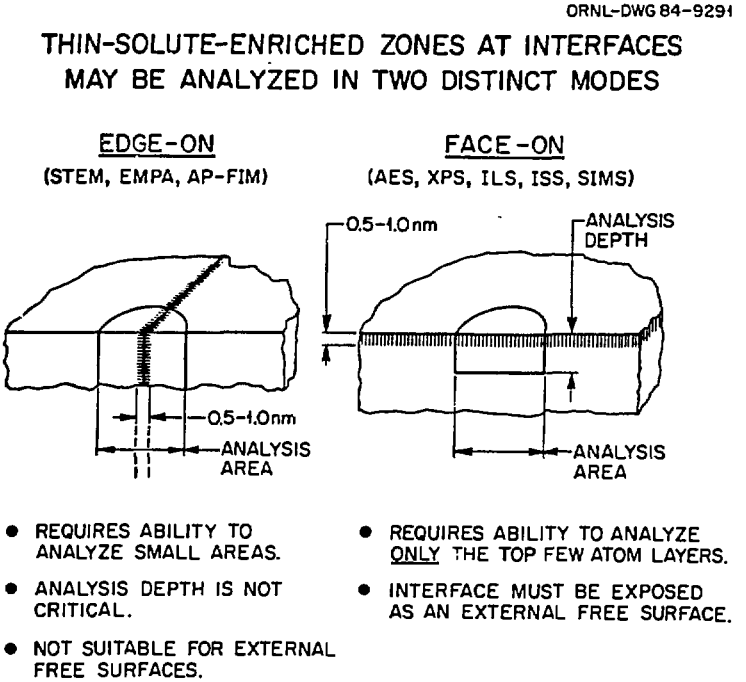

Fig. 2. Schematic illustration showing two distinct modes of interfacial analysis.

ORNL-DWG 84-18341

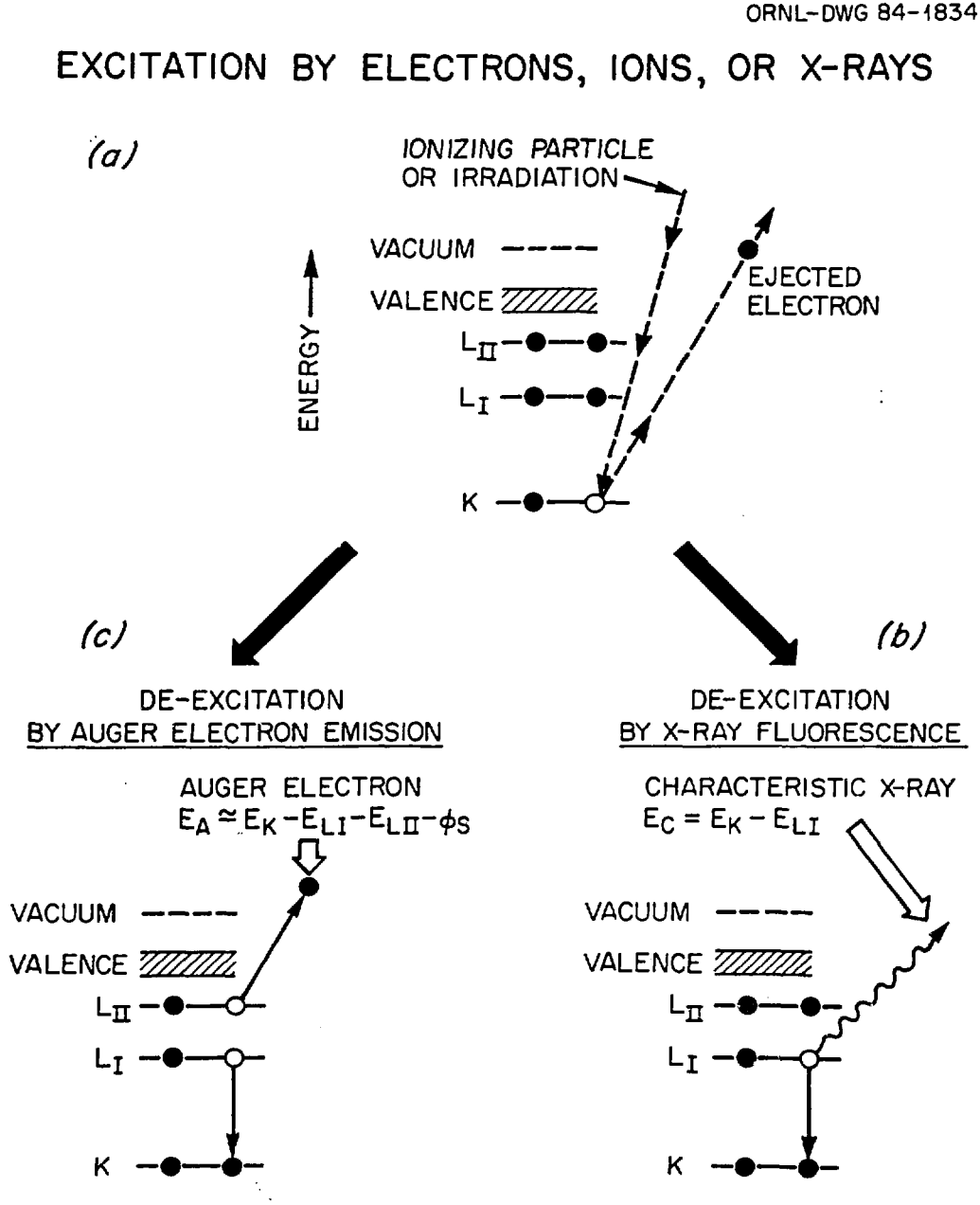

Fig. 3. Comparison of the Auger transition with the more familiar process of x-ray fluorescence.

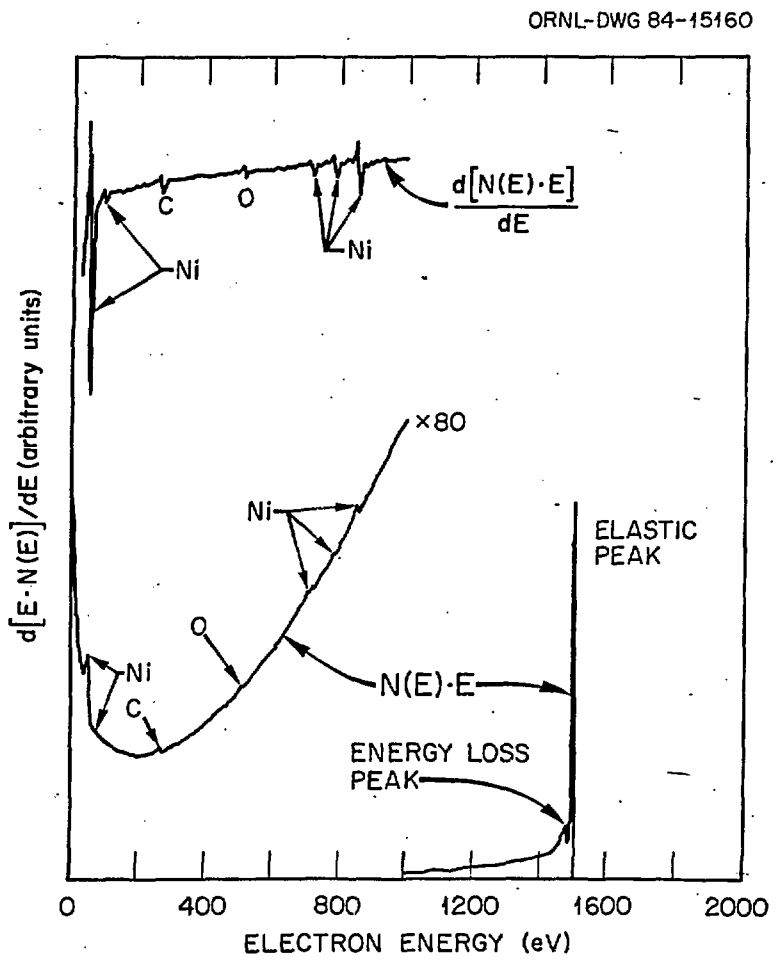

Fig. 4. Secondary electron spectra from a Ni alloy, obtained using a cylindrical mirror analyser (CMA).

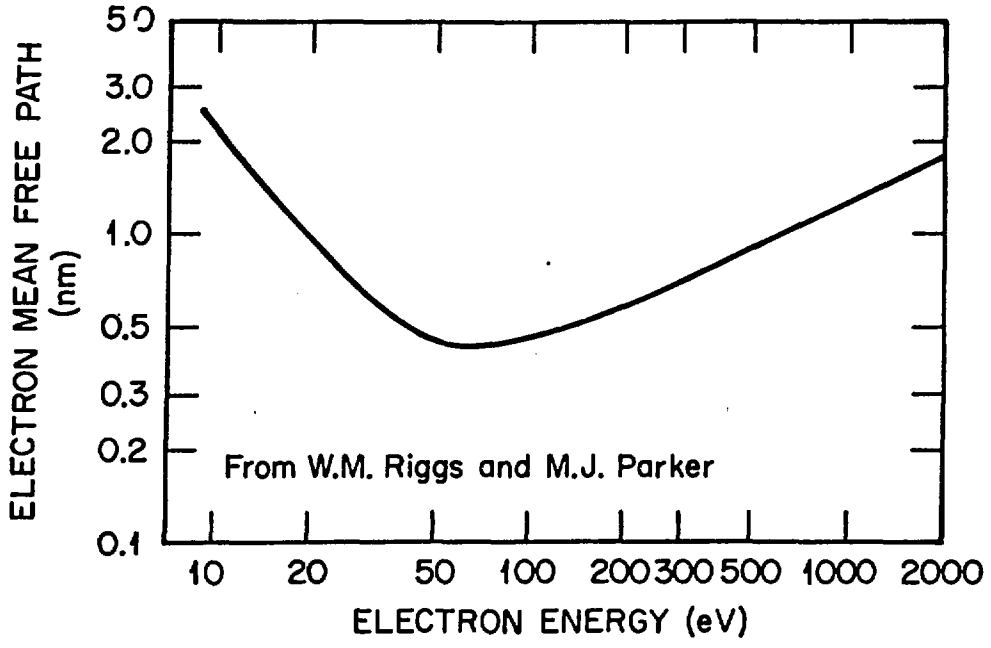

Fig. 5. Plot of the inelastic electron mean free path as a function of electron energy, after Riggs and Parleer (24).

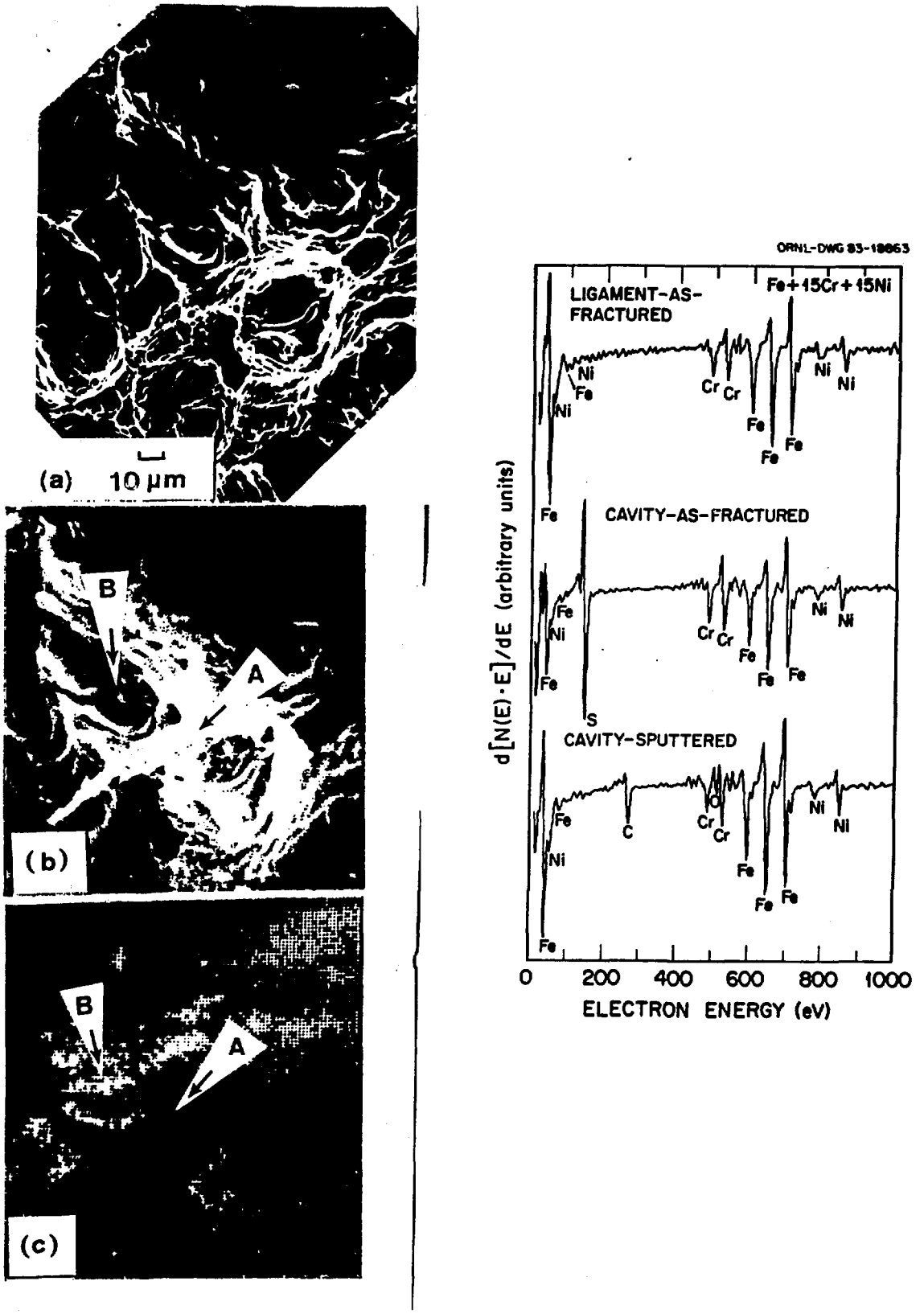

Fig. 6. Conventional scanning electron micrograph (*a*), secondary electron image (*b*), sulfur map (*c*) and Auger spectra (*d*) of a creep cavitated austenitic steel that was fractured in the AES analysis chamber to expose creep cavity surfaces [*B* in (*b*)] and transgranular rupture of intercavity ligaments [*A* in (*b*)].

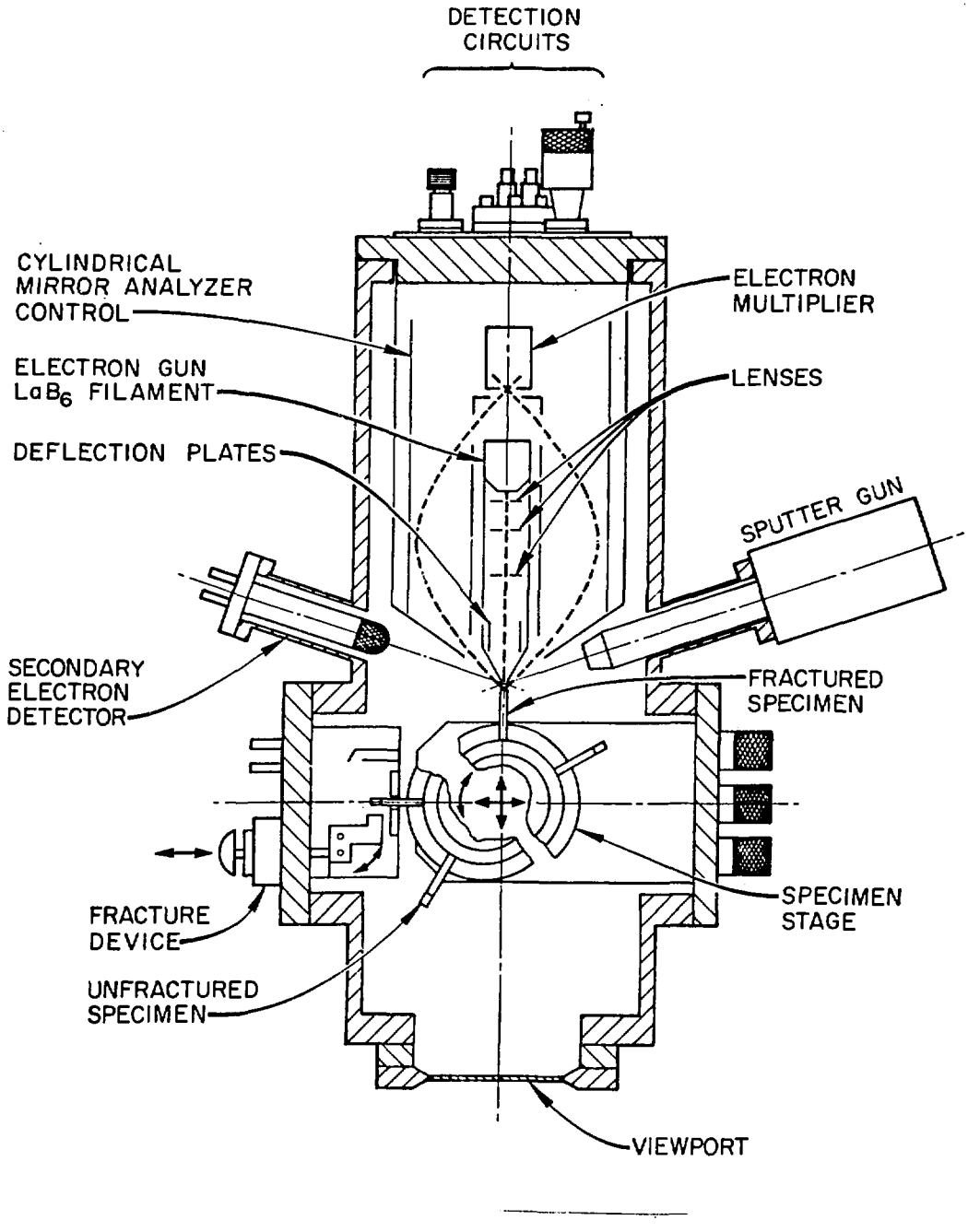

Fig. 7. Schematic view of a conventional AES analysis chamber incorporating a cylindrical mirror analyser (CMA) with a coaxial scanning electron gun. Curved dashed lines show the electron trajectory through the CMA.

ORNL-DWG 84-15158

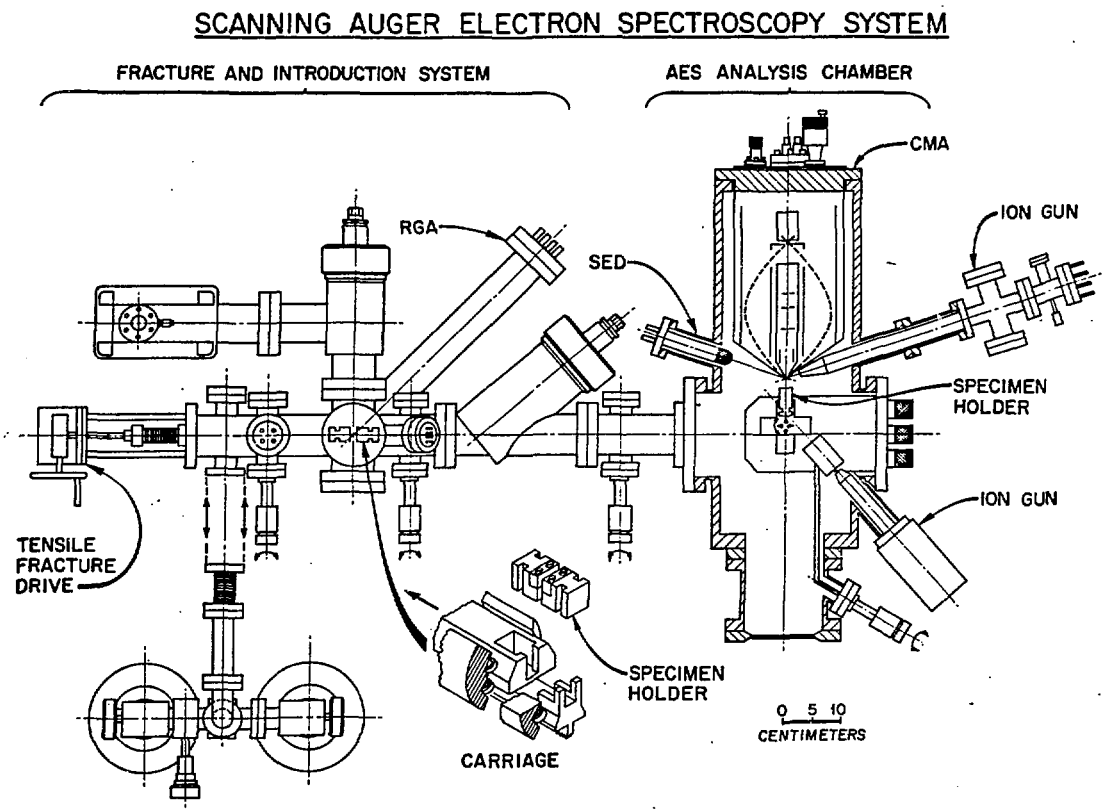

Fig. 8. Schematic view of a more complex AES system, based on the analysis chamber in Fig. 7.

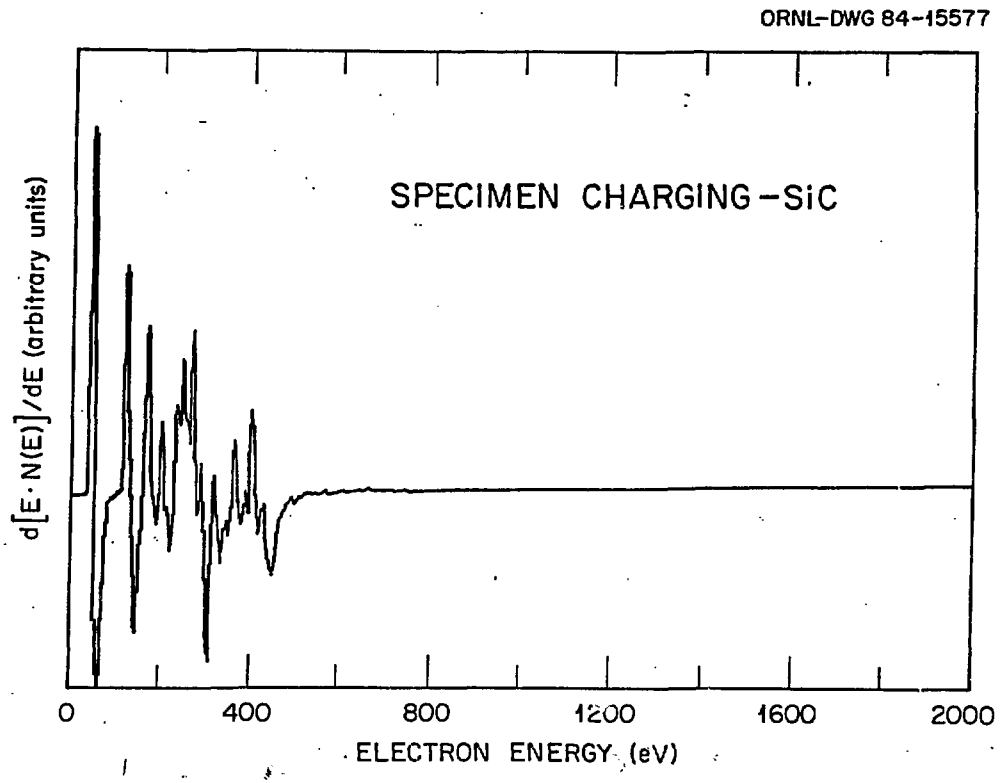

Fig. 9. Typical secondary electron spectrum from an electrically insulating specimen exhibiting charging.

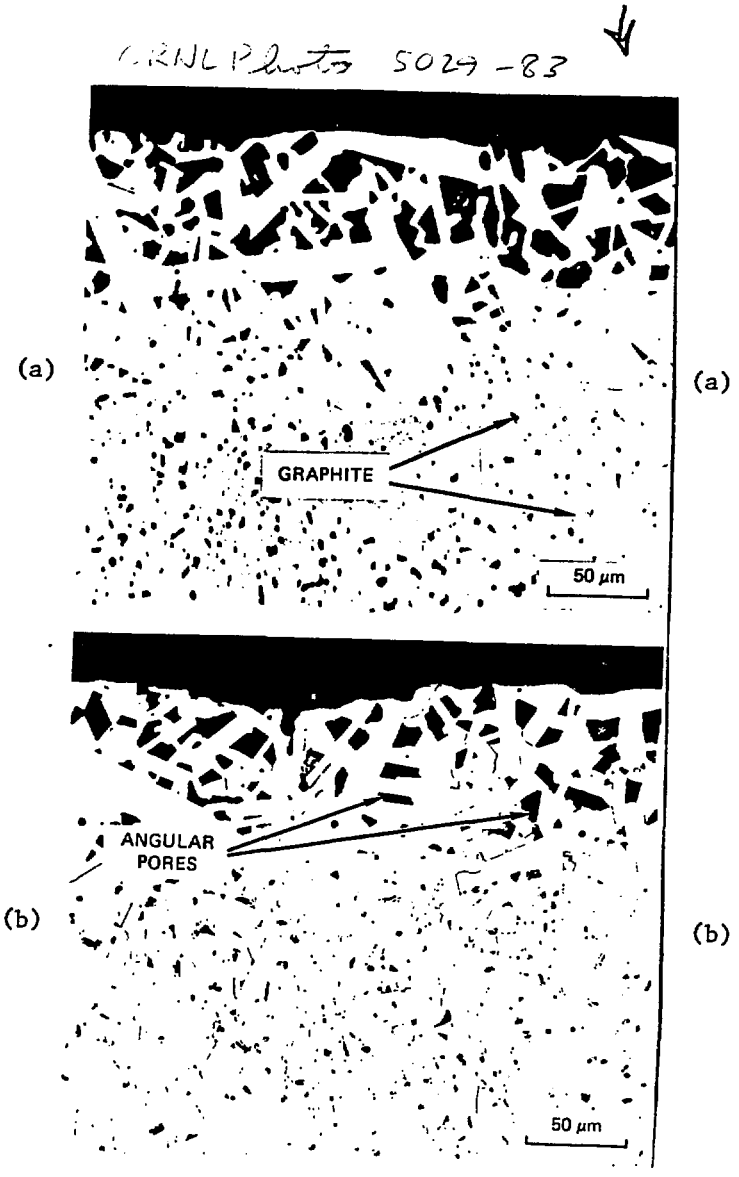

Fig. 10. Optical micrograph of sintered α-SiC tubes exposed to a steel soaking pit environment.

ORNL-PHOTO 5958-84

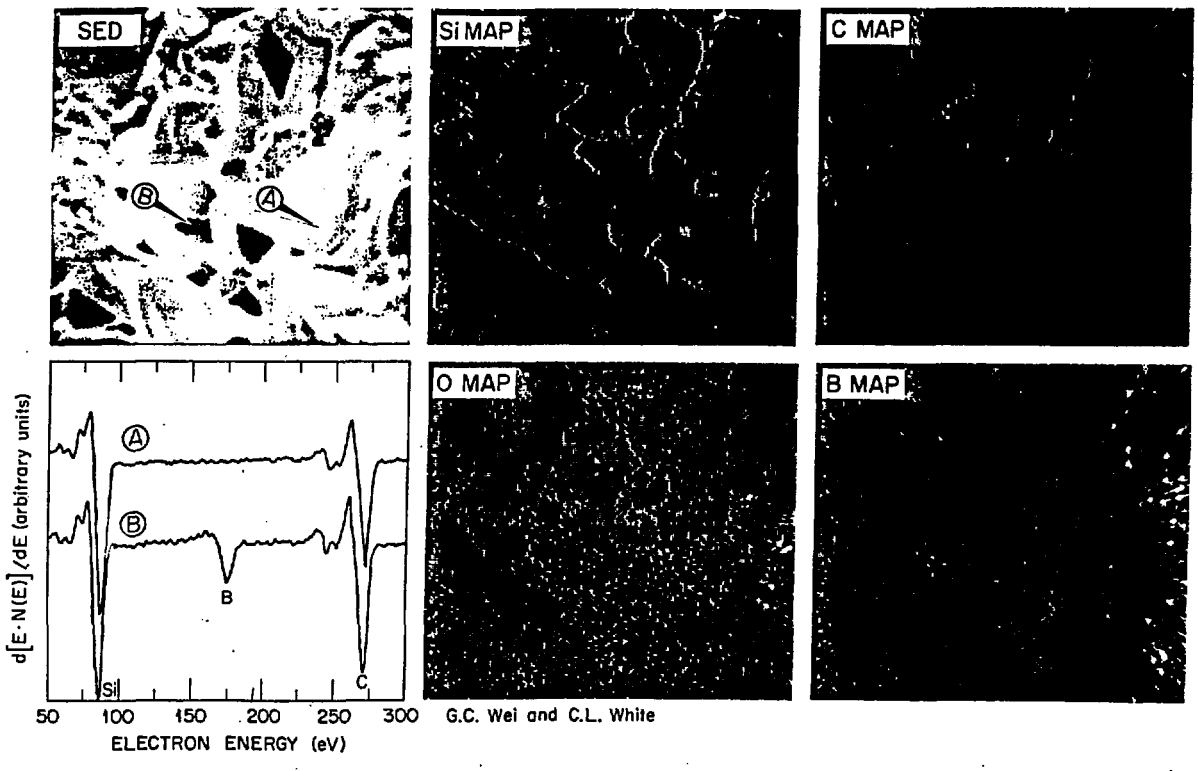

Fig. 11. AES analysis of fractured α-SiC tubes in Fig. 10.

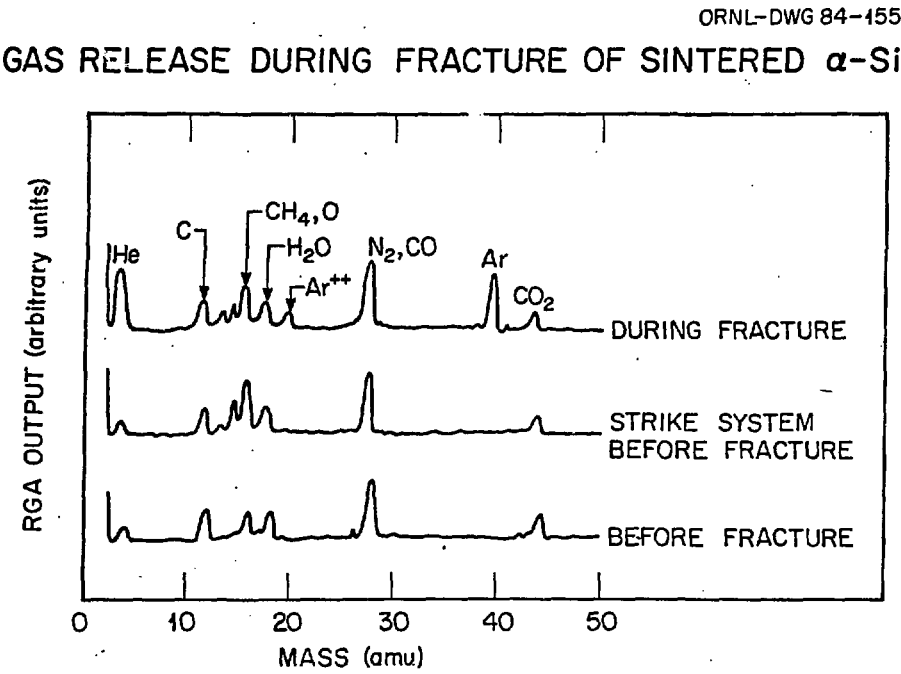

Fig. 12. Residual gas analyser (RGA) spectrum taken during fracture of the α-SiC tubes in Figs. 10 and 11. The bottom curve shows the RGA spectrum before fracture, and the middle spectrum illustrates the effect of striking the system without fracturing the specimen.

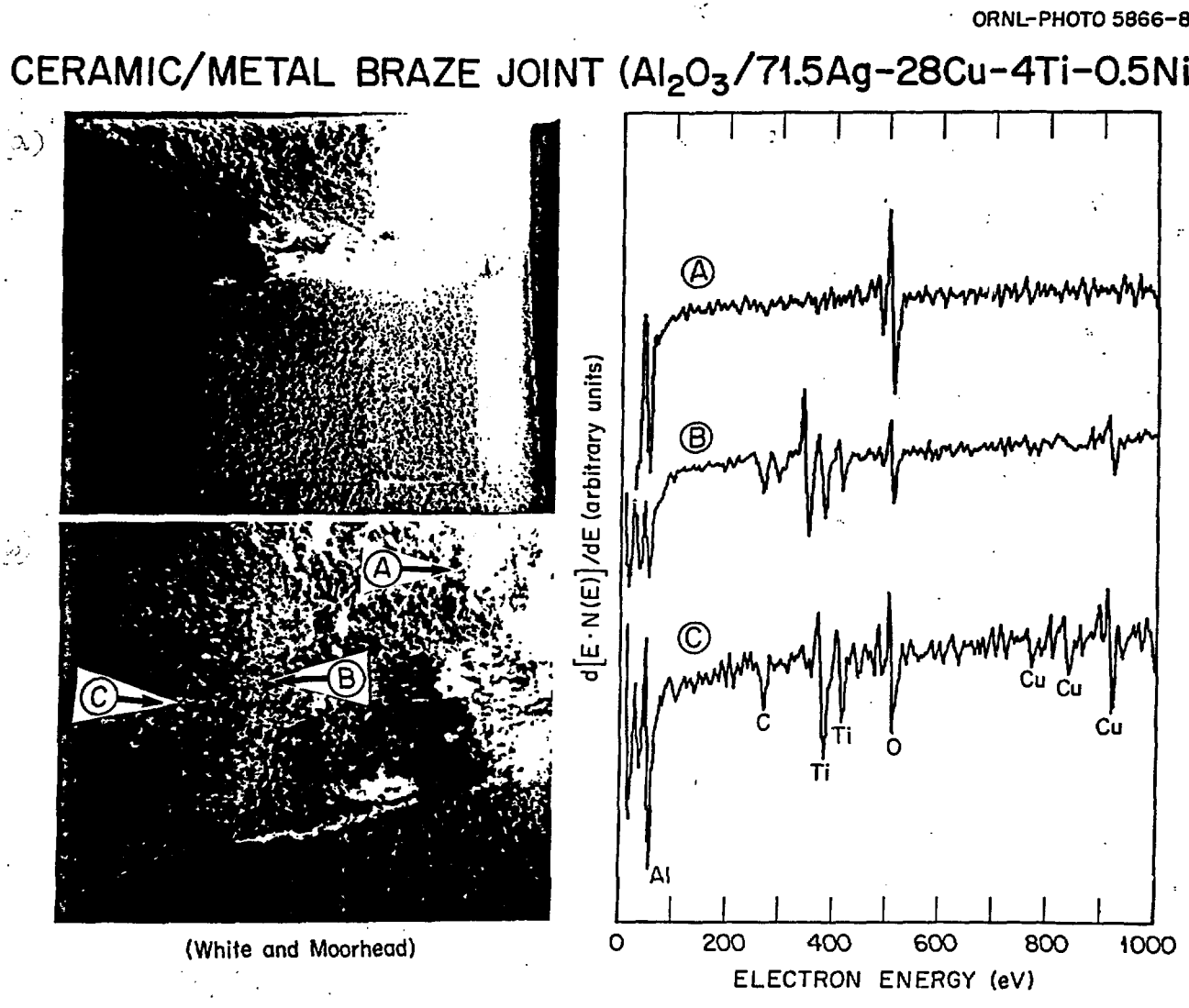

Fig. 13. AES analysis of a fractured ceramic/metal (Al_2O_3/71.5 Ag - 28 Cu - 4 Ti - 0.5 Ni) braze joint after removal of ≈13 nm by sputter etching. Secondary electron detector (SED) images (a) and (b) show locations where Auger spectra (c) were obtained.

Fig. 13 14

ORNL-PHOTO 5865-84

CERAMIC/METAL BRAZE JOINT
(Al_2O_3/71.5Ag-28Cu-4Ti-0.5Ni)

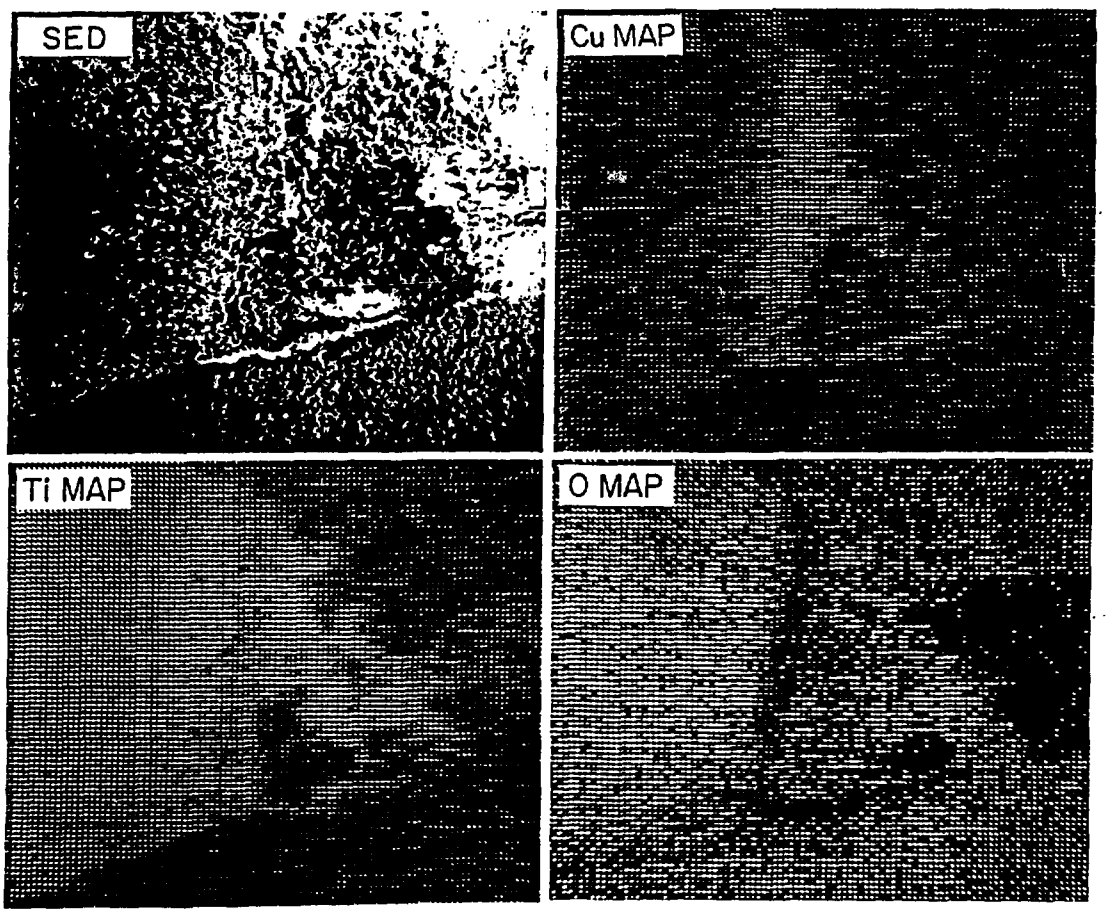

Fig. 14. SED image and Cu, Ti, and O maps of the fractured braze joint in Fig. 13.